Volume 1 | Number 1 | Jan 2013 | Pages 1–100

Analytical Methods

www.rsc.org/methods

ROYAL SOCIETY OF CHEMISTRY

ROYAL SOCIETY OF CHEMISTRY

www.rsc.org/methods

1
2
3
4
5
6
7
8
9
10
...

Graphical Abstract

The ØNHOH@p-MWCNT immobilized on GCE through simple electrochemical cycling technique showed well defined surface confined redox peaks for the stabilized ØNHOH intermediate species and electrocatalysis for NADH at 0.02 V vs Ag/AgCl.

In Situ Stabilization of Hydroxylamine via Electrochemical Immobilization of 4-Nitrophenol on Carbon Nanotube Modified Electrodes: NADH Electrocatalysis at Zero Potential†

Sornambikai Sundaram,[ab] Annamalai Senthil Kumar, [a] Madhanagopal Jagannathan [b] and Mohammed Rafiq Abdul Kadir [*b]

[a] *Environmental and Analytical Chemistry Division, School of Advanced Sciences, Vellore Institute of Technology University, Vellore-632104, India.*

[b]*Medical Implant Technology Group (MEDITEG), Faculty of Biosciences and Medical Engineering, Universiti Teknologi Malaysia (UTM), 81310 UTM Skudai, Johor Bahru, Johor, Malaysia. E-mail: rafiq@biomedical.utm.my; Fax: +60 7 5526222; Tel: +60 7 5535961*

1

Electrochemical immobilization of 4-nitrophenol (4-NP) was conducted on a purified multi-walled carbon nanotube (p-MWCNT) modified glassy carbon electrode (GCE/p-MWCNT) in pH 7 phosphate buffer solution (PBS). The electrochemical reduction of 4-NP to stable in situ electrogenerated aminophenol (ØNHOH) intermediate species within the p-MWCNT matrix may be the underlying mechanism of immobilization. The ØNHOH-stabilized p-MWCNT modified electrode, GCE/ØNHOH@p-MWCNT, showed stable and well-defined surface-confined redox peaks at -0.11 V (A1/C1) and 0.080 V (A2/C2) vs Ag/AgCl over other CNT-modified GCEs. The modified electrode system suggested quasi-reversible and reversible electron transfer mechanisms for the A1/C1 and A2/C2 redox couples. TEM analysis of ØNHOH@p-MWCNT hybrid powder demonstrated the presence of ØNHOH species on the surfaces, as well as inner walls of the p-MWCNTs. XRD peaks exhibited shifts in the 2θ values for the hybrid material compared with the unmodified materials, which confirmed the stabilization of ØNHOH within the p-MWCNT via π-π interactions. Electrochemical characterization of the GCE/ØNHOH@p-MWCNT revealed two electron transfer mechanisms with adsorption-controlled and Nernstian behaviours. A highly sensitive electrocatalytic oxidation of dihydronicotinamide adenine dinucleotide (NADH) at 0.02 V vs Ag/AgCl was achieved with the GCE/ØNHOH@p-MWCNT. Furthermore, the hybrid electrode successfully sensed NADH amperometrically with 2.9 nA/µM sensitivity, a 0.043 µM limit of detection and a linear detection range of 100 µM to 1 mM for ten successive additions of 100 µM NADH at an applied potential of 0.02 V vs Ag/AgCl in pH 7 PBS.

Nitrophenols (NPs) are one of the major organic toxic pollutants exposed to the environment from chemical industries according to the US Environmental Protection Agency and Agency for Toxic Substances and Disease Registry (ATSDR).[1-3] Therefore, numerous studies have been conducted concerning the adsorption and detection of NPs as analytes using different techniques.[4-9] However, these reports involved time-consuming and expensive adsorption/detection procedures.[4-9] Moreover, the catalytic reduction of 4-NP to 4-aminophenol (4-AP) is an irreversible process that proceeds relatively slowly in the absence of a catalyst.[4] Recently, our group has demonstrated rapid and reversible electrochemical methods for the immobilization of various phenol-based organic compounds via the stabilization of electrogenerated intermediate species onto carbon nanotube (CNT) modified glassy carbon electrodes (GCEs).[10-13] The phenolic hydroxyl groups and the *ortho-* or *para-* carbons of the aromatic ring play key roles in such immobilization processes. In addition, the aromatic nitro groups, along with the phenolic groups, can easily be reduced electrochemically to form aminophenols.[14] However, the formation of thin films using AP was reported to be a difficult task: the amino group present in AP gets oxidized easily at higher anodic potentials due to the chain coupling reaction during continuous electrochemical cycling of the polymeric film.[15] Therefore, in this work, in situ electrogenerated 4-AP (hydroxylamine,ØNHOH) intermediate species were stabilized via 4-NP immobilization onto the purified multi-walled CNT (p-MWCNT) matrix-modified GCE under a lower anodic potential by a rapid and simple electrode preparation procedure.

Previous studies on the electrochemical behaviour of 4-NP on various modified electrodes used higher reduction/oxidation potentials, a portion of which exhibited feeble redox peaks.[15-24] To the best of our knowledge, there are no findings on (i) 4-NP chemically modified

3

redox-mediated systems stabilized via ØNHOH intermediate species within the CNT matrix through simple preparation procedures and (ii) GCE/ ØNHOH@p-MWCNTs for sensing the biological analyte dihydronicotinamide adenine dinucleotide (NADH). Therefore, in this work, a ØNHOH@p-MWCNT hybrid material was prepared electrochemically, characterized physico- and electro-chemically and applied to the electrocatalysis of NADH in pH 7 phosphate buffer solution (PBS).

The experimental section in the Electronic Supplementary Information (ESI)† gives details about chemicals, instrumentation, electrode preparation and sample preparation methodologies. The surface coverage of the immobilized 4-NP, $\Gamma_{\text{ØNHOH}}$ (μmol.cm^{-2}), was determined from a cyclic voltammogram (CV) by integrating the anodic peak area (Q_a) of the respective redox peak at $v = 50$ mV.s^{-1} taken from the last cycle and calculated using the equation $\Gamma_{\text{ØNHOH}} = Q_a/nFA$, where n is the number of electrons $(n = 2)$, and A is the geometric surface area (0.0707 cm^2).

(Figure 1)

Initially, the electrochemical experiments on the GCE/MWCNT in 1 mM 4-NP at 50 mV.s^{-1} were carried out in two different potential windows: the long window (-0.5 to 1.0 V vs Ag/AgCl) and the short window (-0.2 to 0.6 V vs Ag/AgCl) in pH 7 PBS. Potential cycling was initiated from the negative potential towards the positive potential throughout this work. The CV responses obtained for three different potential cycles are shown in Fig. 1A. Initially, no peak was observed in the short window even after continuous potential cycling (Fig. 1A(a)). However, when the potential window was extended to the long range as mentioned above, in the 1st cycle of film formation, two oxidation peaks at 0.369 V (A') and 0.8 V (A1') in the anodic direction and two reduction peaks at 0.025 V (C2) and -0.282 V (C') in the cathodic direction were

4

observed, as shown in Fig. 1A(b). Furthermore, growth in the peak currents from the 3rd cycle at potentials -0.050 V (A1, a hump), 0.047 V (A2) and 0.480 V (A') in the anodic and -0.055 V (C1, a hump), 0.028 V (C2) and -0.39 V (C') in the cathodic direction were observed (Fig. 1A(c)) in addition to the A1' peak as mentioned above. To remove the loosely bound 4-NP molecules, the electrode was washed and the medium was transferred to blank PBS then subjected to continuous potential cycling. Interestingly, the two redox couples A1/C1 (-0.025 V/-0.080 V) and A2/C2 (0.065 V/0.029 V) were observed to remain on the electrode surface. Furthermore, decreases in the peak current for the A', A1' and C' irreversible peaks were observed for the medium-transferred electrode as shown in Fig. 1A(d) (the 20th cycle of the stabilization process is given in the figure). The arrow marks in Fig. 1A represent the peak current direction with increases in the potential cycles. In this figure, decreases in the A', A1' and C' peak currents and increases in the A1, C1, A2 and C2 peak currents were observed with an increasing number of potential cycles. This phenomenon was quite similar to the CV peaks reported by Yang on a SWCNT-modified GCE electrode, which was carried out previously in the potential window of -0.5 to 1.0 V in pH 5.0 PBS.[17] Moreover, the previous study also reported that, when the cathodic sweep was reversed before -0.72 V under the same conditions, the redox couple at 0.11 V disappeared. Yang explained that the electrochemically reduced species of 4-NP at -0.72 V was responsible for the appearance of the redox couple at the positive potential in his work.[17]

Meanwhile, to determine the underlying electrochemical reactions for the appearance of the redox couples in this work, various potential window segments were investigated based on the higher peak current and redox peak separation values. *Note: the CV responses of the potential window optimization are not given here.* During electrochemical cycling in the potential window of -0.6 to 0.6 V vs Ag/AgCl, we observed the appearance of two A1/C1 and A2/C2 redox

5

couples with well-resolved peak potentials and higher peak currents. Based on the above findings, the potential window of -0.6 V to 0.6 V was chosen as an optimal window for further electrochemical experiments. The comparative CV responses of the GCE/MWCNT in 1 mM 4-NP solution (curve a) and the medium-transferred 4-NP immobilized GCE/MWCNT (curve b) after 20 continuous cycles in the optimal potential window are given in Fig. 1B. In Fig. 1B(a) initially, during the 1st CV cycle, there was no peak observed in either the anodic or cathodic directions. However, when the number of potential cycles was increased, small oxidation peaks in the anodic direction at -0.095 V (A1) and 0.074 V (A2) appeared, followed by the appearance of reduction humps at -0.228 V (C'), -0.079 V (C1) and 0.076 V (C2) from the 4th cycle onwards. After 10 continuous potential cycles, we observed well-resolved peaks for the A1/C1 redox couple at -0.098 V/-0.11V and A2/C2 redox couple at 0.08 V/0.06 V. The calculated peak-to-peak separation ($\Delta E_p = E_{pa}-E_{pc}$, pa and pc corresponding to the anodic and cathodic peak currents) values were 0.012 ± 0.007 V for A1/C1 and 0.02 ± 0.001 V for A2/C2. The calculated apparent standard electrode potential ($E^{o\prime} = (E_{pa}+E_{pc}) / 2$) values were 0.104 ± 0.01 V and 0.07 ± 0.001 V for the A1/C1 and A2/C2, respectively. In addition, the calculated ratios between the anodic and cathodic peak current (i_{pa}/i_{pc}) were 0.77 and 1.08 for A1/C1 and A2/C2, respectively. These peaks revealed the presence of a quasi-reversible electron transfer mechanism for the A1/C1 and a reversible electron transfer mechanism for the A2/C2 redox couple with 4-NP, which acted as a redox mediator for the GCE/MWCNT in this work. Furthermore, it was interesting to notice that both the A1/C1 and A2/C2 redox peaks were still retained on the medium-transferred GCE/ØNHOH@MWCNT electrode surface with a relative standard deviation (RSD) of 2.7% (taken for the last 10 out of 20 cycles) along with the C'

irreversible peak (Fig. 1B(b)). However, no such electron transfer behaviour was observed for

the bare GCE in the present study (data not shown).

(Scheme 1)

Based on the above findings, the oxidation peaks at A' and A1' in Fig. 1A may be

assigned to the irreversible oxidation of 4-NP as reported by Yin et al.[25] at 0.9 V for the

GCE/hydroxyapatite nanopowder in pH 7 PBS. The shift in the oxidation peak potential in this

work to 0.8 V from 0.9 V may be due to the change in the supporting matrix. Further, both the

reduction peaks observed at -0.1 V in Fig. 1A and 1B may be assigned to the reduction of $-NO_2$,

and the oxidation peaks at 0.095 V and 0.074 V may be assigned to the $-OH$ group present in 4-

NP.[15,16] Meanwhile, the reduction peak C' at ~ -0.3 V vs Ag/AgCl may be assigned to the nitryl

functional group.[20] According to the literature, the electrochemical behaviour of 4-NP follows a

proposed reaction pathway as given in Scheme 1 for pH 5.0 to 7.0. In the first step, nitrophenol is

reduced to hydroxyl aminophenol along with the transfer of four electrons and four protons, from

where the irreversible reduction peak of nitryl was derived. In the second step, the hydroxyl

aminophenol removes one H_2O to yield benzoquinoneimine, which can lose two electrons to

form aminophenol as an end product. Following the above mentioned pathway in this work, the

hydroxyl aminophenol can be captured by the well-defined pores of the MWCNT and be

oxidized at the catalytic active site of GCE/MWCNT to *para*-(hydroxyamino)phenol-*para*-

nitrosophenol. This reaction is a reversible reaction with two electrons and two protons

transferring to 4-AP, leading to the formation of the A1/C1 and A2/C2 redox couples.[15,16,18,20,26-

30] Thus in this work, the ØNHOH peak electrogenerated during the 4-NP immobilization was

subsequently stabilized within the MWCNT interface through π-π interaction, resulting in two

stable redox peaks at A1/C1 (-0.011 V) and A2/C2 (0.08 V).

7

Meanwhile, to optimize a suitable CNT matrix for the immobilization of 4-NP, to determine the influence of the metal, metal oxide and carbonaceous impurities present and the significance of the number of tubular walls in the CNT matrix, different types of CNTs were subjected to similar electrochemical studies in this work, as shown in Fig. 1B. The "as commercially received" impure MWCNT, f-MWCNT (f=functionalized), p-MWCNT (p=purified) and SWCNT were compared. The CV responses of the different CNT-modified GCEs for 4-NP immobilization are given in the ESI† Fig. S2A and its interpretation are discussed in the ESI†. To further confirm the redox mechanism of ØNHOH, the electrochemical behaviour of bare 4-AP was studied with the optimal p-MWCNT matrix-modified GCE under optimal experimental conditions. Interestingly, the bare 4-AP also showed similar qualitative redox behaviours at -0.05 V (A1/C1) and 0.15 V (A2/C2) as shown in the ESI† Fig. S1A. This observation was in agreement with the literature report for the redox couple at ~0.11 V vs Ag/AgCl on *para*-aminophenol-MWCNT-TiO$_2$ electrode and on *para*-aminophenol-CNT carbon paste electrode at pH 6.0.[31,32] Meanwhile, when 3-NP, an isomer of 4-NP, was subjected to electrochemical immobilization on GCE/p-MWCNT, no redox behavior was noticed (ESI† Fig. S1B). Thus, in this study, the proposed electrode was selective for the immobilization of the 4-NP isomer. These results suggested that the presence of a nitro functional group in the 4th position of the benzene ring led to the formation of ØNHOH intermediate species, which, in turn, assisted the immobilization of nitrophenol in agreement with our earlier finding.[10] Furthermore, to assess the formation of the ØNHOH@p-MWCNT hybrid and its position in the p-MWCNT matrix, the ØNHOH@p-MWCNT samples were analysed by XRD and TEM.

The XRD patterns of the ØNHOH@p-MWCNT (c), 4-NP (a) and p-MWCNT (b) powder samples are displayed in the ESI† Fig. S3. The XRD peaks observed at 2θ =11.51, 21.75, 25.75,

29.78, 35.99º and 44.06 for the ØNHOH@p-MWCNT powder sample showed a mixture of characteristic crystalline 4-NP and amorphous p-MWCNT XRD peaks. A slight shift in the 2θ peak values were noticed for the hybrid material when compared with the bare powders. This shift might be due to the π-π interaction between the aromatic ring of the intermediate species of 4-NP (ØNHOH) and the sp^2 hexagonal carbon of the p-MWCNT along the inner walls of the nanotubes.[33] A combination of low-abundance and broad peaks could render the crystalline peak undetectable by XRD. Therefore, some of the 4-NP characteristic peaks that were noticed in the native 4-NP with lesser intensity might have been hidden in the wavy XRD peak pattern of the ØNHOH@p-MWCNT hybrid powder. The TEM micrographs of the ØNHOH@p-MWCNT powder obtained at different magnifications are given in Figs. 2A and 2B. Black spots were noticed on the outer surface and along the inner side walls of the CNT in addition to a swollen nanotube structure for the p-MWCNT at some locations in the morphology. Based on the CV results obtained, the electrogenerated ØNHOH species might have diffused into or penetrated inside the walls of the CNT and settled there via strong π-π molecular bonding along with fractions of the CNT surface-bound ØNHOH species. This observation was quite similar to what we observed in our earlier findings on the immobilization of amoxicillin onto the CNT matrix.[33]

(Figure 2)

To further confirm the presence of the redox-active sites within the CNT matrix, the ØNHOH@p-MWCNT powder sample prepared for XRD analysis was subjected to electrochemical study under the optimal experimental conditions. The powder sample was selected for this study because the powder was thoroughly water washed, so no CV response was expected. A 2 mg of the p-MWCNT was dispersed in 500 µL of ethanol, from which a 3µL aliquot was drop-coated on the cleaned GCE and then subjected to potential cycling (ESI† Fig.

S4). There was no peak appearance in the first cycle until the formation of the A' and A1' peaks,

which may have arisen due to the wet-air oxidation of the –OH functional group.[10] However,

starting from the 2nd run, feeble A1/C1 and large A2/C2 redox peaks along with the C' reduction

peak appeared and remained constant even after prolonged CV cycles (ESI† Fig. S4). This CV

response of the solution-phase prepared ØNHOH@p-MWCNT powder was qualitatively similar

to the response of the in situ prepared electrode in this study, even after the removal of loosely

bound 4-NP. This similarity suggested the existence of fractions of nitrophenol and ØNHOH

units within the 4-NP+p-MWCNT mixture systems. These fractions of ØNHOH@p-MWCNT

might have occurred due to the reduction of 4-NP to 4-AP in the absence of any catalyst[4] and

stabilized into the matrix when treated electrochemically. The fractions of stabilized

ØNHOH@p-MWCNT units resulted in the formation of A1/C1 and A2/C2 redox peaks in the

CV of the ØNHOH@p-MWCNT powder-modified electrode. The calculated $\Gamma_{ØNHOH}$ values for

the solution-phase prepared ØNHOH@p-MWCNT powder-modified GCE were 16 $\mu mol.cm^{-2}$

for the A2/C2 redox couple and 12 $\mu mol.cm^{-2}$ for the A1/C1 redox couple. These values were

~9.4 and 9.8 times lower than 149.60 and 117.62 $\mu mol.cm^{-2}$ $\Gamma_{ØNHOH}$ values for A1/C1 and

A2/C2, respectively, obtained for the electrochemically prepared GCE/ØNHOH@p-MWCNT.

This observation in turn confirmed the presence of the redox mediator active site inside the walls

of the CNT.

(Figure 3)

To understand the possible mechanism involved in the electron-transfer reaction on the

GCE/ØNHOH@p-MWCNT, the electrode was examined for the effects of scan rate and solution

pH. The effect of scan rate on the CV response of the medium transferred GCE/ØNHOH@p-

MWCNT in pH 7 PBS is shown in Fig. 3A. There was a systematic increase in the peak current

values with respect to the scan rate varying from 5-500 mV.s^{-1}. Linear plots were drawn between log i_{pa} and $v^{1/2}$ which resulted in slope ($\partial \log i_{pa}/\partial v^{1/2}$) values of 1±0.8 for the A1 and A2 peaks as shown in the Fig. 3B. This slope value is close to the ideal value for the adsorption-controlled electron transfer mechanism. A plot between the current function ($i_f = i_{pa}/v^{1/2}$) and the scan rate showed an exponential increase in the current function as given in Fig. 3C, which confirmed the adsorption-controlled electron transfer mechanism for the A1/C1 and A2/C2 redox processes on the GCE/ØNHOH@p-MWCNT. This trend was in agreement with the XRD, TEM and electrochemical characterization of the ØNHOH@p-MWCNT powder samples and the observations of the interaction between the intermediate species and the inner walls of the p-MWCNT matrix. This interaction might have led to the occurrence of surface-confined redox peaks. The typical CV responses of a GCE/ØNHOH@p-MWCNT in solution pHs varying from 3 to 10 at a scan rate of 50 mV.s^{-1} are shown in Fig. 3D. The redox peak currents were found to increase as pH increased from 3 to 7, and thereafter, a drastic decrease in the peak current values were noticed. A similar finding was reported by Yin et al.[25] with the highest peak current achieved for pH 7 when the pH was varied between 3 and 11. In agreement with the literature, the A1/C1 and A2/C2 redox couple in the present work also showed the maximum peak current in pH 7 PBS.[25] In addition, a shift in the peak potentials was also observed from the positive to the negative end of the potential windows for the of A1/C1 and A2/C2 redox peaks with the increase in the solution pH . Calibration plots for $E_{1/2}$ vs pH are shown as inset figures in Fig. 3E & 3F, which yielded slope ($\partial E_{1/2}/\partial pH$) values of 0.060 ± 0.01 V.pH^{-1} and 0.060 ± 0.05 V.pH^{-1}. The slope values were close to an ideal value of 0.059 V.pH^{-1} for the Nernstian redox behaviour with involvement of equal numbers of e$^-$ and H$^+$. This system exhibited proton-coupled electron-transfer behaviours of the A1/C1 and A2/C2 redox couples, in agreement with the literature. [26-30]

11

(Figure 4)

(Scheme 2)

The GCE/ØNHOH@p-MWCNT hybrid electrode was further studied for its electrocatalysis behavior for NADH in pH 7 PBS. The electrocatalytic oxidation of NADH (NAD^+/NADH) is of significant research interest as it is needed for regenerating the active form of glutathione, generating ATP, and replenishing the body's energy currency.[34] The electrocatalytic oxidation behaviours of the GCE/ØNHOH@p-MWCNT hybrid electrode (d) in comparison with other unmodified electrodes, GCE (a), and GCE/p-MWCNT (b) in the presence of 500 μM NADH dissolved pH 7 PBS at a scan rate of 10 mV.s^{-1} under optimal experimental conditions are all given in Fig. 4A. The CV response of the GCE/ØNHOH@p-MWCNT in blank pH 7 PBS in the absence of NADH is given in Fig. 4A (c) for comparison. As seen in Fig. 4A, the unmodified electrodes failed to give any NADH oxidation signal. Interestingly, a large peak current signal for the NADH electrocatalytic oxidation was observed on the GCE/ØNHOH@p-MWCNT (d) at 0.02 ± 0.005 V in the location of the A2/C2 redox peak potential. The surface-confined ØNHOH species formed during the electrochemical process on the GCE/p-MWCNT might have acted as redox mediators and interacted with the NADH, resulting in electrocatalysis at 0.02 V. The possible mediated electrocatalysis is illustrated in scheme 2, in agreement with the literature.[30] The amperometric *i-t* responses of the modified electrode (a) in comparison with the GCE (c) and GCE/ p-MWCNT (b) for a 100 μM spike of NADH each are shown in Fig. 4B, where a linear increase in the peak current with respect to the NADH concentration was observed. The calibration plots shown in Fig. 4C(a) for the modified electrode showed 100 μM – 1 mM as the linear range of NADH detection. The linear equation for the amperometric *i-t* response was i (μA) = 2.9±0.001 nA μM^{-1} + 0.2169 ±0.041 μA (R=0.9832) with a calculated

detection limit value of 0.043 µM (based on a signal-to-noise ratio of 3). Meanwhile, there was a non-linear peak current response for consecutive spikes of NADH for the unmodified electrodes, as seen in Figs. 4C (b & c). The obtained results for the sensitivity and lower electrocatalytic oxidation potential for NADH detection have been compared to the results in the literature and are given in table S1 in the ESI†.[2,34-42]

Conclusions

The electrochemical behaviour of 4-nitrophenol on CNT-modified GCEs in neutral pH resulted in specific surface-confined redox peaks on the working electrode. The mechanism for the immobilization of 4-NP onto the CNT matrix-modified GCE might have involved its transformation to hydroxylamine (ØNHOH) intermediate species during electrochemical potential cycling. The proposed hybrid electrode was highly useful for the amperometric *i-t* sensing of NADH at zero electrocatalytic oxidation potential in a neutral pH. The GCE/ØNHOH@p-MWCNT prepared through a simple electrochemical methodology via the immobilization of 4-NP is demonstrated as a chemically modified electrode for the first time in the literature. Further, the electrocatalysis of NADH at zero potential in the neutral pH reported in this work was found to be unique among the past research findings. Finally, the GCE/ØNHOH@p-MWCNT hybrid electrode developed in this work is a potential candidate for the electrochemical sensing of NADH at lower potential and for the adsorption and detection of the high-risk pollutant 4-NP from the environment, if extended in the form of an electrochemical sensor strip for practical applications.

13

Acknowledgments

Notes and references

1. U.S. Environmental Protection Agency, *Health and Environment Effects Profile No. 135*, Washington, DC, 1980.

2. A.K.M. Kafi and A. Chen, *Talanta*, 2009, **79**, 97-102.

3. P. Mulchandani, Y. Lei, W. Chen, J. Wang and A. Mulchandani, *Anal. Chim. Acta*, 2002, **470**, 79-86.

4. T. Selvaraju, J. Das, K. Jo, K. Kwon, C.-H. Huh, T. K. Kim and H. Yang, *Langmuir,* 2008, **24**, 9883-9888.

5. E. Marais and T. Nyokong, *J. Hazard. Mater.*, 2008, **152**, 293-301.

6. J. Ruana, I. Urbe and F. Borrull, *J. Chromatogr A.*, 1993, **655**, 217-226.

7. G. Norwitz, N. Nataro and P.N. Keliher, *Anal. Chem.*, 1986, **58**, 639-641.

8. X. Que, D. Tang, B. Xia, M. Lu and D. Tang, *Anal. Chim. Acta.*, 2014, **830**, 42-48.

9. X. Wu, L. Qiu, Z.Z. Yang and F. Yan, *Appl. Catal A: Gen.,* 2014, **478**, 30-37.

10. S. Sornambikai and A.S. Kumar, *Electrochim. Acta.*, 2012, **62**, 207-217

11. P. Swetha and A.S. Kumar, *Chem. Asian. J.,* 2013, **8**, 896-901.

12. P. Barathi and A.S. Kumar, *Chem. Eur. J.*, 2013, **19**, 2236-2241.

13. A.S.Kumar and P. Swetha, *Colloids Surf., A,* 2011, **384**, 597-604.

14. P. Heiduschka and F. W. Scheller, *Biosens. Bioelectron.,* 1994, **9**, vii-ix.

15. X. Lü, Z. Wu, J. Shen, J. Feng, Y. Wang and Y. Song, *Int. J. Electrochem. Sci.,* 2013, **8**, 2229-2237.

16. Y.-L. Yang, B. Unnikrishnan and S.-M. Chen, *Int. J. Electrochem. Sci.,* 2011, **6**, 3902-3912.

17. C. Yang, *Microchim. Acta*, 2004, **148**, 87-92

18. M.A.El Mhammedi, M. Achak, M. Bakasse and A. Chtaini, *J. Hazard. Mater.,* 2009, **163,** 323-328.

19. A. Chandra Roy, V.S. Nisha, C. Dhand, Md.A. Ali and B.D. Malhotra, *Anal. Chim. Acta,* 2013, **777**, 63-71.

20. T. Zhang, Q. Lang, D. Yang, L. Li, L. Zeng, C. Zheng, T. Li, M. Wei and A. Liu, *Electrochim. Acta*, 2013, **106**, 127-134.

21. Y. Wei, L.-T. Kong, R. Yang, L. Wang, J.-H. Liu and X.-J. Huang, *Langmuir*, 2011, **27**, 10295-10301.

22. J. Das, M.A. Aziz and H. Yang, *J. Am. Chem. Soc.*, 2006, **128**, 16022-16023.

23. T. Selvaraju, J. Das, S. W. Han and H. Yang, *Biosens. Bioelectron.*, 2008, **23**, 932-938.

24. M. Pontie, L. Sikpo, G. Thouand, R. Lahan, I. Tapsoba, R. Mallet and T. Feng, *Electroanalysis*, 2011, **23**, 433-441.

25. H. Yin, Y. Zhou, S. Ai, X. Liu, L. Zhu and L. Lu, *Microchim. Acta*, 2010, **169**, 87-92.

26. L.-Q. Luo, X.-L. Zou, Y.-P. Ding and Q.-S. Wu, *Sens. Actuators, B.*, 2008, **135**, 61-65

27. Y. Tang, R. Huang, C. Liu, S. Yang, Z. Lu and S. Luo, *Anal. Methods*, 2013, **5**, 5508-5514.

28. K. Giribabu, R. Suresh, R. Manigandan, S. Munusamy, S. P. Kumar, S. Muthamizh and V. Narayanan, *Analyst*, 2013, **138**, 5811-5818.

29. R. Madhu, C. Karuppaiah, S.-M. Chen, P. Veerakumar and S.-B. Liu, *Anal. Methods*, 2014, DOI: 10.1039/c4ay00795f.

15

30. M. Santhiago, P.R. Lima, W.de Jesus R. Santos, A.B. de Oliveira and L.T. Kubota, *Eletrochim. Acta*, 2009, **54**, 6609-6616.

31. A.A. Ensafi, E. Khoddami, B. Rezaei and H. Karimi-Maleh, *Colloids Surf. B*, 2010, **81**, 42-49.

32. A.A. Ensafi, S. Dadkhah-Tehrani and H. Karimi-Maleh, *Anal. Sci.*, 2011, **27**, 409-414.

33. A.S. Kumar, S.Sornambikai, T.L. Deepika and J.-M. Zen, *J. Mater.Chem.,* 2010, **20**, 10152-10158.

34. A.A. Ensafi, H. Karimi-Maleh and S. Mallakpour, *Colloids. Surf., B*, 2013, **104,** 186-193.

35. J. Chen, J. Bao, C. Cai and T. Lu, *Anal. Chim. Acta*, 2004, **516**, 29-34.

36. C.E. Banks and R.G. Compton, *Analyst*, 2005, **130**, 1232-1239.

37. M. Musameh, J. Wang, A. Merkoci and Y. Lin, Low, *Electrochem. Commun.*, 2002, **4,** 743-746.

38. K.-C,Lin, Y.-S. Li and S.-M. Chen, *Sens. Actuators, B.*, 2013, **184**, 212-219.

39. J. Zheng, W. Wei, L. Wu, X. Liu, K. Liu and Y. Li, *J. Electroanal. Chem.*, 2006, **595**, 152-160.

40. C. Deng, J. Chen, X.L. Chen, C.Xiao, Z.Nie and S.Yao, *Electrochem. Commun*., 2008, **10**, 907-909.

41. J.P. Metters, F. Tan, R.O. Kadara and C.E. Banks, *Anal. Methods*, 2012, **4**, 3140-3149.

42. J.P. Metters, S.M. Houssein, D.K. Kampouris and C.E. Banks, *Anal. Methods*, 2013, **5**, 103-110.
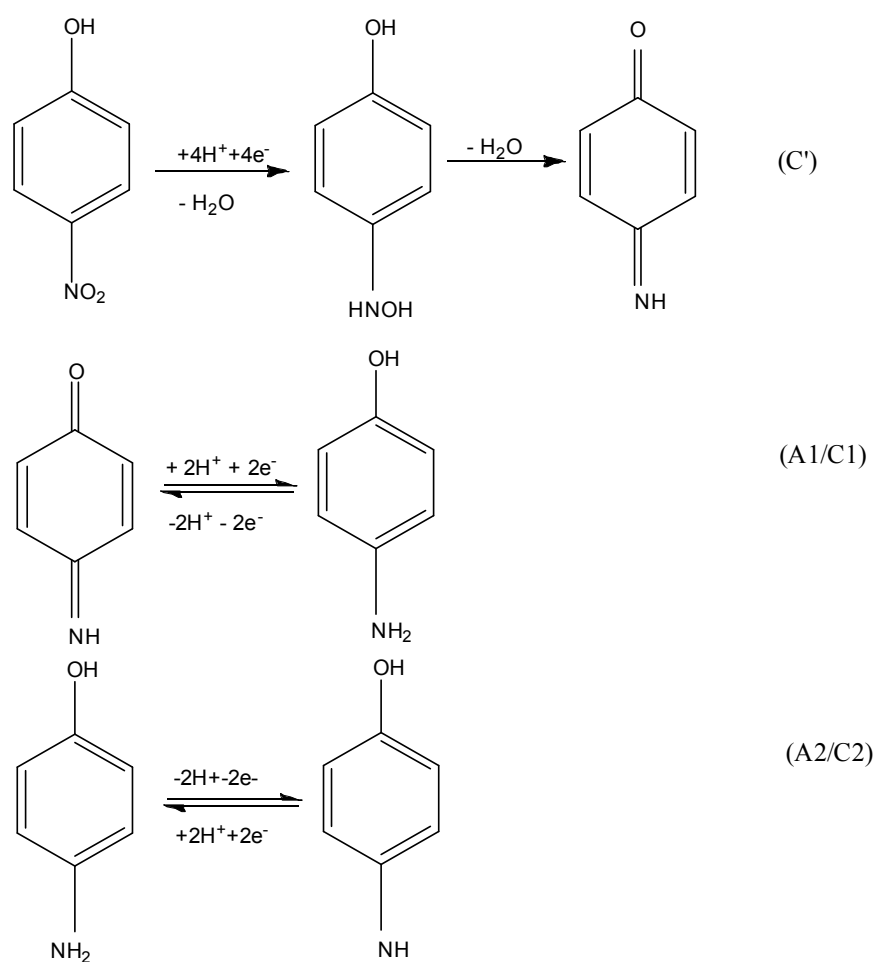
Scheme. 1 Proposed 4-nitrophenol electron transfer mechanism and its intermediate species, showing the hydroxylamine formation involved in the electrochemical behaviour. [20,26-30]

17
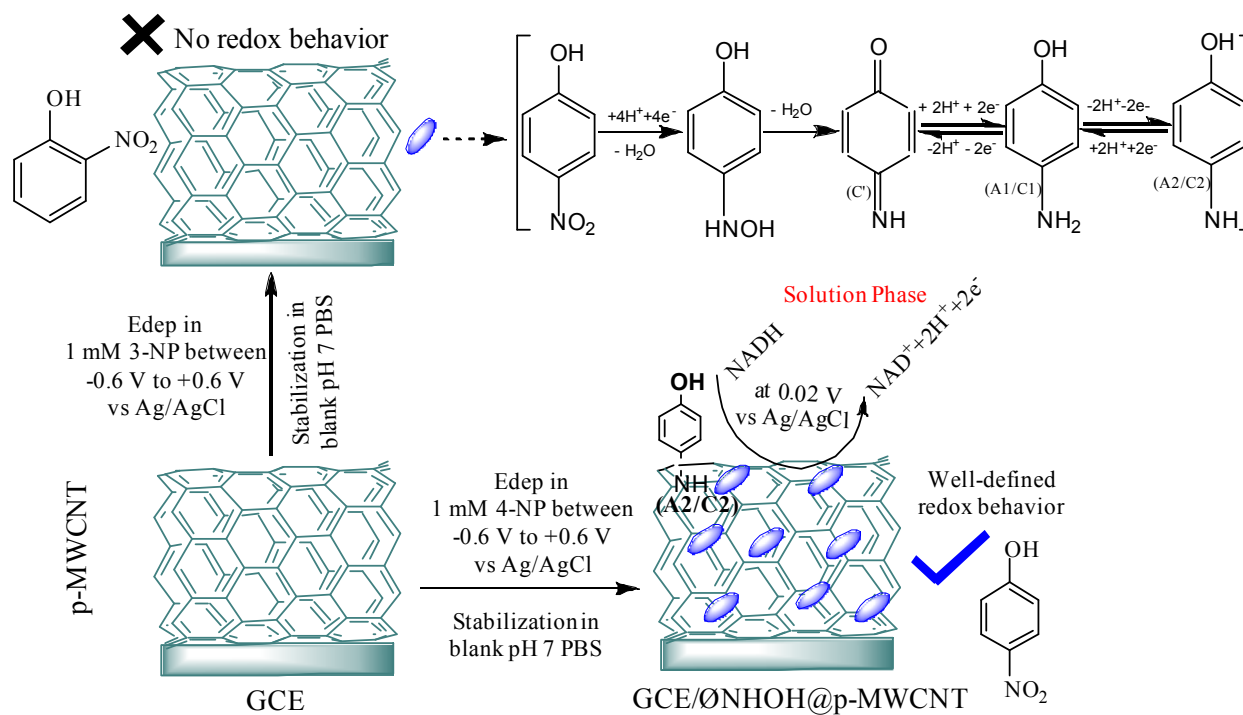
**Scheme. 2** Schematic representation for the electrochemical immobilization of 4-nitrophenol on the CNT electrode surface through the ØNHOH species stabilization process and its electrocatalytic NADH oxidation steps.
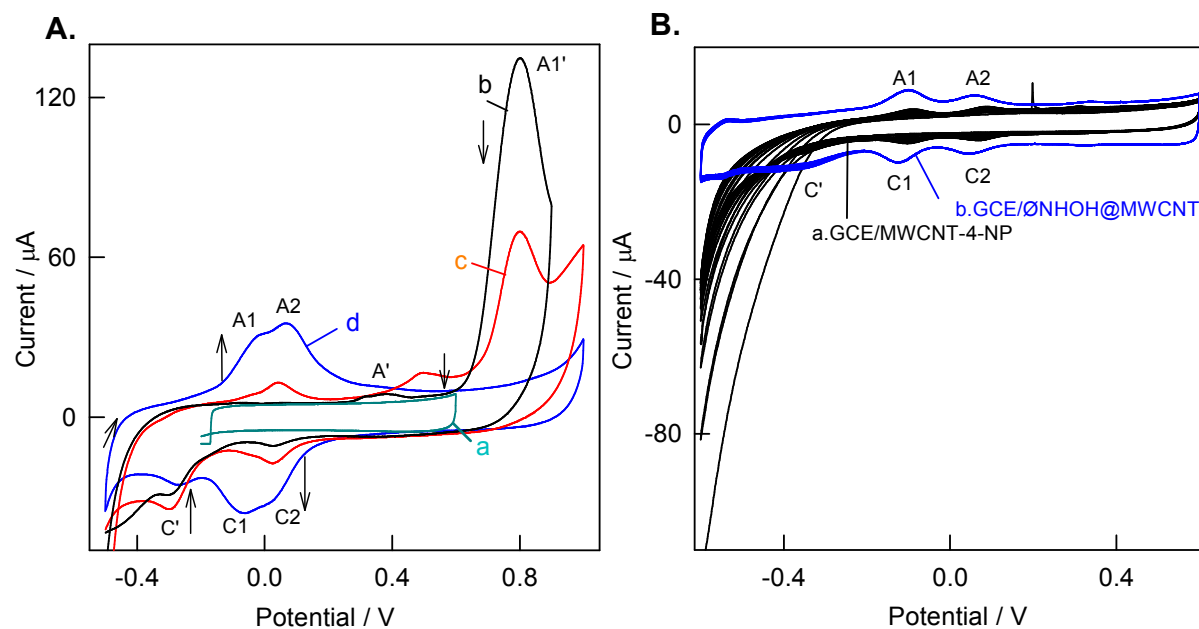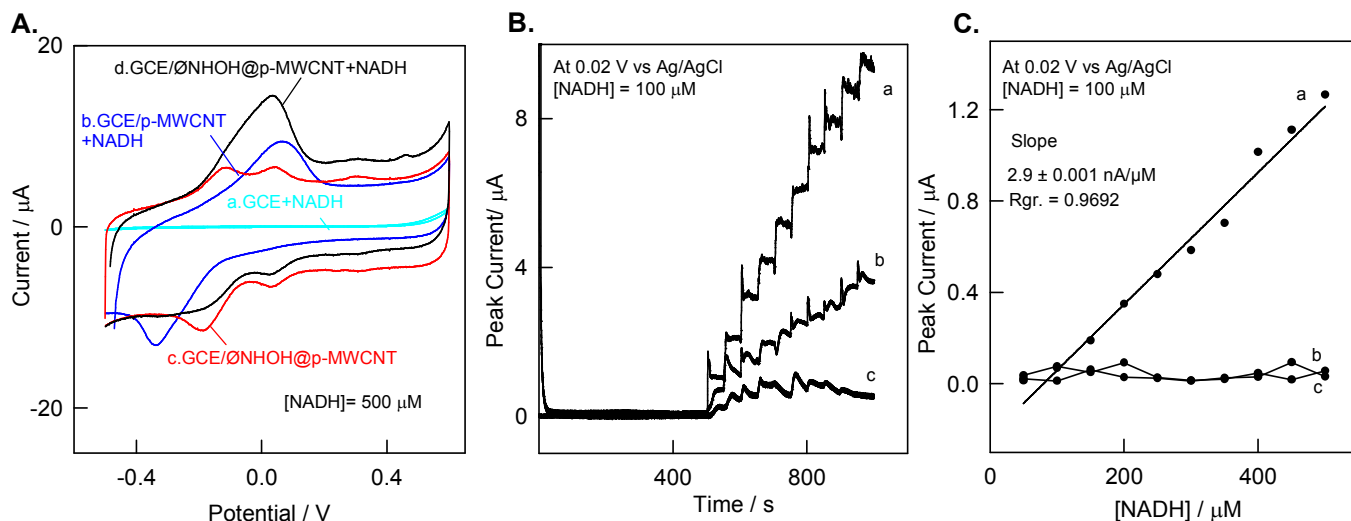
Fig. 1 (A) First-cycle CV responses of the GCE/MWCNT in the short window (a) in comparison with the GCE/MWCNT in 1 mM 4-NP solution for the 1st cycle (b) and 3rd cycle (c) in the long window, 20th cycle CV response of the medium transferred GCE/ØNHOH@MWCNT (d) in the long potential window. (B) 20 continuous CV response of the GCE/MWCNT in 1 mM 4-NP solution (a) in comparison with the ØNHOH immobilized GCE/MWCNT (b) in the potential window of -0.6 V and 0.6 V vs Ag/AgCl. All data correspond to a scan rate of 50 mV.s^{-1} in pH 7 PBS. *Note: The arrow mark represents the peak current direction with respect to the increase in potential cycles.*
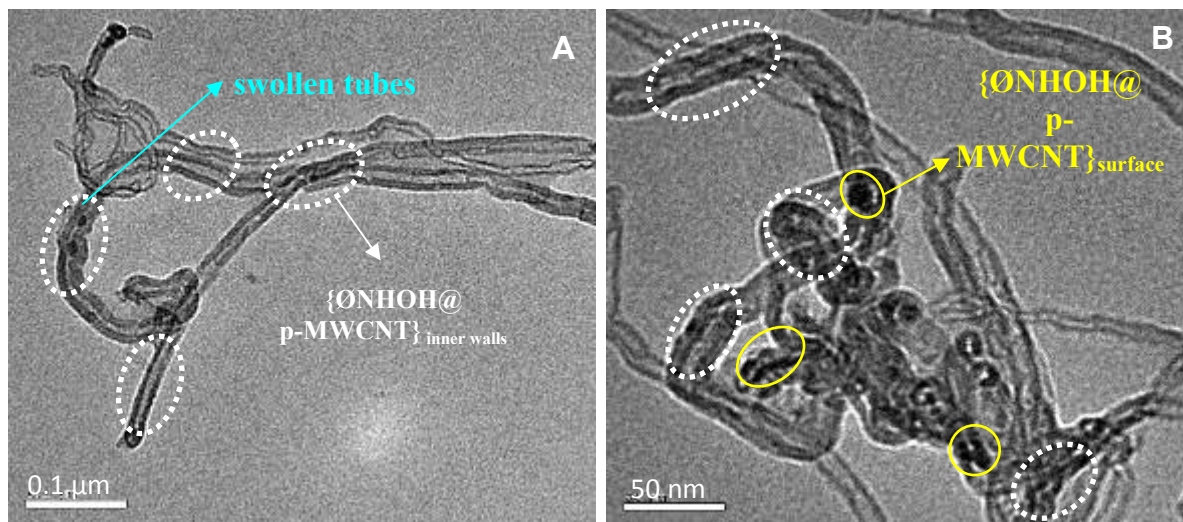
Fig. 2 TEM photographs of the ØNHOH@p-MWCNT powder at 0.1 µm (A) and 50 nm (B) magnifications.
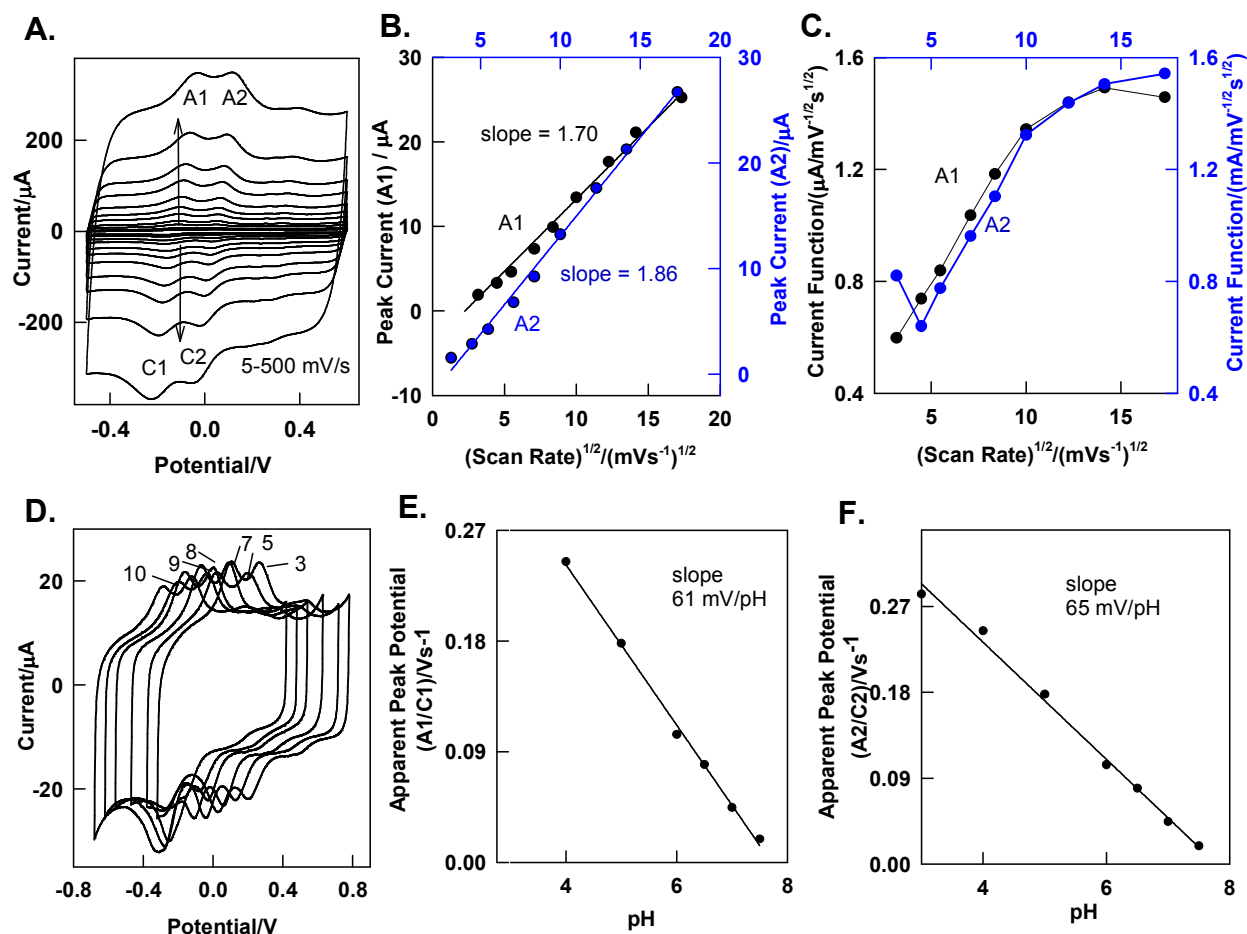
Fig. 3 CV responses for the 10th cycle of the GCE/ØNHOH@p-MWCNT for (A) Different scan rates and (D) Different pH, Calibration plots for the peak current vs square root of the scan rate for the A1 and A2 peak (B), Plots between the current function (i_f) of the A1 and A2 peaks vs square root of the scan rate (C) and Calibration plots of the apparent potential of the redox couple A1/C1 (E) and A2/C2 (F) vs pH.

A.

d.GCE/ØNHOH@p-MWCNT+NADH

b.GCE/p-MWCNT
+NADH

a.GCE+NADH

c.GCE/ØNHOH@p-MWCNT

[NADH]= 500 µM

Current / µA

Potential / V

B.

At 0.02 V vs Ag/AgCl
[NADH] = 100 µM

a

b

c

Peak Current / µA

Time / s

C.

At 0.02 V vs Ag/AgCl
[NADH] = 100 µM

Slope

2.9 ± 0.001 nA/µM
Rgr. = 0.9692

a

b
c

Peak Current / µA

[NADH] / µM

Fig. 4 (A) CV responses for the 10th cycle of GCE/ØNHOH@p-MWCNT (d), bare GCE (a) and GCE/p-MWCNT (b) in the presence of 500 µM NADH in comparison with the GCE/ØNHOH@p-MWCNT (c) in the absence of NADH all at scan rate of 10 mV.s^{-1}, (B) Comparative amperometric *i-t* responses of GCE/ØNHOH@p-MWCNT (a), GCE/p-MWCNT (b) and GCE (c) for 100 µM each spike of NADH under hydrodynamic condition at an applied potential of 0.02 V vs Ag/AgCl and (C) Comparative calibration plots for the peak current vs [NADH] for the GCE/ØNHOH@p-MWCNT (a), GCE/p-MWCNT (b) and GCE (c). Figures (A)-(C) were all obtained for pH 7 PBS electrolytes.